



**HAL**  
open science

# Fractional Entropy of Multichannel Kondo Systems from Conductance-Charge Relations

Cheolhee Han, Andrew K Mitchell, Zubair Iftikhar, Yaakov Kleeorin, Anne Anthore, Frédéric Pierre, Yigal Meir, Eran Sela

► **To cite this version:**

Cheolhee Han, Andrew K Mitchell, Zubair Iftikhar, Yaakov Kleeorin, Anne Anthore, et al.. Fractional Entropy of Multichannel Kondo Systems from Conductance-Charge Relations. *Physical Review Letters*, 2022, 10.1103/PhysRevLett.128.146803 . hal-03432279

**HAL Id: hal-03432279**

**<https://hal.science/hal-03432279>**

Submitted on 17 Nov 2021

**HAL** is a multi-disciplinary open access archive for the deposit and dissemination of scientific research documents, whether they are published or not. The documents may come from teaching and research institutions in France or abroad, or from public or private research centers.

L'archive ouverte pluridisciplinaire **HAL**, est destinée au dépôt et à la diffusion de documents scientifiques de niveau recherche, publiés ou non, émanant des établissements d'enseignement et de recherche français ou étrangers, des laboratoires publics ou privés.

# Extracting entropy of exotic quasiparticles from conductance measurements

Cheolhee Han,<sup>1</sup> Andrew K. Mitchell,<sup>2,3</sup> Z. Iftikhar,<sup>4</sup> Yaakov Kleeorin,<sup>5</sup> A. Anthore,<sup>4,6</sup> F. Pierre,<sup>4</sup> Yigal Meir,<sup>7</sup> and Eran Sela<sup>1</sup>

<sup>1</sup>*Raymond and Beverly Sackler School of Physics and Astronomy, Tel Aviv University, Tel Aviv 69978, Israel*

<sup>2</sup>*School of Physics, University College Dublin, Belfield, Dublin 4, Ireland*

<sup>3</sup>*Centre for Quantum Engineering, Science, and Technology, University College Dublin, Belfield, Dublin 4, Ireland*

<sup>4</sup>*Université Paris-Saclay, CNRS, Centre de Nanosciences et de Nanotechnologies (C2N), 91120 Palaiseau, France*

<sup>5</sup>*Center for the Physics of Evolving Systems, University of Chicago, Chicago, IL, 60637, USA*

<sup>6</sup>*Université de Paris, C2N, 91120 Palaiseau, France*

<sup>7</sup>*Department of Physics, Ben-Gurion University of the Negev, Beer-Sheva, 84105 Israel*

(Dated: August 31, 2021)

Fractional entropy is a signature of nonlocal degrees of freedom, such as Majorana zero modes or more exotic non-Abelian anyons. However, in the mesoscopic quantum systems hosting these states direct entropy measurements remain highly challenging. Here we introduce a self-consistent framework to extract entropy from existing experimental conductance measurements. Applying this approach to conductance measurement through a metallic quantum dot displaying ‘charge’ Kondo effects, we extract the fractional entropy in the two- and three-channel Kondo effects, corresponding to Majorana and Fibonacci zero modes, respectively. In these cases, the entropy extracted from the experimental data falls on a theoretical curve displaying scaling towards  $k_B \log \sqrt{2}$  or  $k_B \log \frac{1+\sqrt{5}}{2}$  entropy, respectively. Our protocol provides a general route towards a direct extraction of entropy from charge measurements in mesoscopic quantum systems.

A plethora of condensed-matter systems are conjectured to support exotic quasi-particles, which may serve as basic ingredients for quantum technologies [1]. However, whether these particles have been observed experimentally is currently the topic of a vivid debate. For example, current experimental evidence for the observation of Majorana fermions (MFs) is based on measurements of zero-bias peaks in the differential conductance which, however, can be attributed also to various other sources [2]. By contrast, thermodynamic quantities can unambiguously separate MFs from other, simpler excitations [3–5]. Specifically, the additional entropy due to a single Majorana fermion is given by  $S = \frac{1}{2}k_B \log 2$ . This entropy is half of that of a spin-degenerate state, suggesting that information is stored non-locally across a pair of bound states that are decoupled from one another. This non-locality is hard to identify in a conductance measurement. However, the fractional contribution to the entropy is conceptually clear and, importantly, it cannot be attributed to a degenerate localized excitation. The measurement of a fractional entropy therefore would serve as a smoking-gun signature for exotic quasi-particles [6, 7].

The difficulty with measurements of thermodynamic quantities in general, and entropy in particular, is that techniques developed for measuring thermodynamic behaviour in bulk materials are in general not applicable to engineered lower-dimensional systems, where changes in signal are simply too minute, due to the small number of electrons contributing to any effect and the relatively large background contributions from the phonon bath. Therefore, characterisation through thermodynamic signatures of intriguing states of matter that have shown to emerge in such low-dimensional electron systems remains challenging. Recently entropy of mesoscopic devices has been measured through either employing the Maxwell relation [8], which relates the temperature dependence of the charge occupation of the device,  $dN/dT$ , to the gate-voltage dependence of the entropy, or through thermopower measurements [9].

Here we demonstrate that standard conductance measurements can be utilized to extract the entropy of the system when charge-occupation measurements are not available (see Fig. 1). In many cases, the theory is characterized by a single energy scale, such as the charging energy in the Coulomb blockade regime or the Kondo temperature in Kondo systems. Then theory predicts a universal relation between  $dN/dT$  and conductance  $G$ . (In some of the cases described below, such as the Coulomb blockade regime or the two-channel Kondo effect, they are both proportional to the density of states and thus to each other.) Using such a relation, obtained from theory of a given model, the experimental value of the fractional entropy of the quasiparticles can be extracted from the conductance measurement. This also serves as a consistency check on the theory, as the theory predicts independently the value of that entropy.

In the following, we focus on multi-channel Kondo (MCK) systems [10] which support exotic quasi-particle in their ground states. The model describes  $k$  channels of conduction electrons interacting antiferromagnetically with an impurity spin  $\frac{1}{2}$ . The impurity entropy  $S_{\text{imp}}$  is defined as the extra entropy of the system associated with the impurity. Consider first the single-channel case. While the weakly coupled impurity has double degeneracy with  $S_{\text{imp}} = \log 2$  (here and below we set the Boltzmann constant to unity), the antiferromagnetic coupling leads to a spin-singlet formation between the impurity and the Fermi sea at temperatures lower than the Kondo temperature  $T_K$ , resulting in a non-degenerate ground state and zero entropy. However, when multiple  $k$  channels of conduction electrons interact

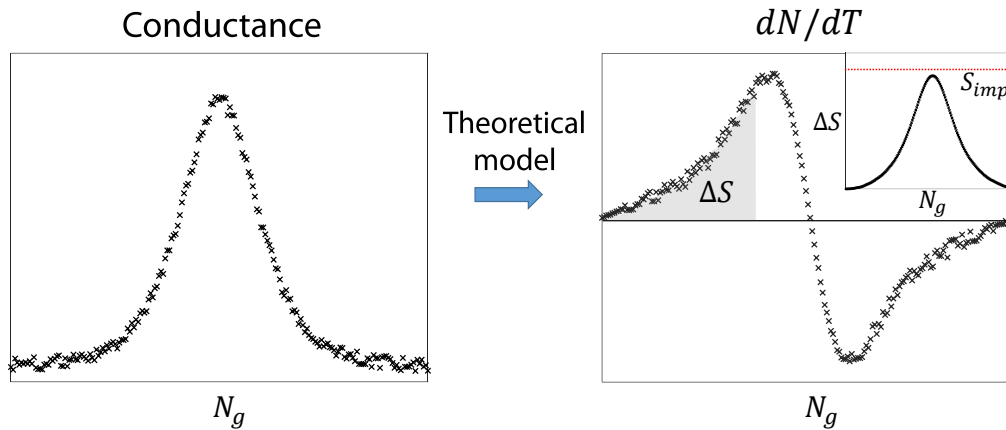


Figure 1. **Illustration of the method.** Left panel: Experiment provides conductance data versus gate voltage (here randomly generated for illustration). Using a theoretical relation between  $dN/dT$  and the conductance (e.g. Eq.(3), Eq.(5), or Fig. 4b), one can extract  $dN/dT$  from experimental conductance (right panel). The entropy difference can be obtained by integrating over  $dN/dT$  (shaded region). The inset shows the extracted entropy, and the maximum corresponds to the entropy of the quasi-particle.

equally with the impurity spin, spin-singlet formation is prevented, resulting in a non-Fermi liquid (NFL) state with nontrivial impurity entropy  $S_{\text{imp}} = \log \{2 \cos [\pi/(2+k)]\}$  [11–13]. These predicted fractional values of the impurity entropy correspond to a ground-state zero mode, such as a MF in the two-channel Kondo (2CK) case [14], where  $S_{2\text{CK}} = \log \sqrt{2}$ , or a Fibonacci anyon in the three-channel Kondo (3CK) case, where  $S_{3\text{CK}} = \log \frac{1+\sqrt{5}}{2}$ . Thus MCK systems promise an alternative, gapless platform [15, 16] for MFs and non-abelian anyons [17–19].

The charge 2CK and 3CK effects were demonstrated in a metallic quantum dot (QD) in the quantum Hall regime, connected between two or three spinless leads [20, 21], respectively (see inset in Fig. 2(b)), coupled to  $k$  leads by quantum point contacts (QPCs) [20–26]. Each QPC consists of a pair of counter-propagating spinless fermions (due to the large magnetic field), one incoming into the QD and the other outgoing from the QD. The Hamiltonian of the model is

$$H = \hbar v_F \sum_{j=1}^k \sum_{\nu=\text{in,out}} \int dx \psi_{j\nu}^\dagger i \partial_x \psi_{j\nu} + E_C (\hat{N} - N_g)^2 + \hbar v_F \sum_{j=1}^k r_j \psi_{j\text{in}}^\dagger(0) \psi_{j\text{out}}(0) + \text{h.c.} \quad (1)$$

This model maps onto the anisotropic  $k$  channel MCK model [20–22]. The first term in  $H$  describes the free fermion modes  $\psi_{j\nu=\text{in,out}}$ , with  $v_F$  the Fermi velocity, and the last term describes a reflection  $r_j$  at the various QPCs, which we assume were tuned to be equal  $r_j \equiv r$ , except where we discuss the crossover between different regimes.  $E_C$  is the charging energy and  $\hat{N}$  is the electron number operator of the QD. The reflection amplitude  $r$  is related to the transmission coefficient  $\tau$  as  $1 - \tau_j \simeq r_j^2$  [27, 28]. The transmission  $\tau$  in turn determines the Kondo temperature  $T_K$ . If  $\tau$  is small, then the system is in the classical Coulomb blockade (CB) regime ( $T \gg T_K$ ), and if  $\tau$  is enhanced, and the temperature lowered below a  $\tau$ -dependent  $T_K$ , then the system exhibits the 2CK or 3CK behaviour depending on the number of the coupled channels.  $N_g$  is the gate voltage applied to the metallic dot, normalized to unity when an additional electron is added to the dot, which corresponds to a magnetic field in the spin Kondo models. The charge degeneracy at the Coulomb peaks (at  $N_g = 1/2$ ) maps to an effective impurity spin [24] and by tuning the gate voltage, the crossover between NFL and FL is realized. The MCK models were found to accurately describe the experimental QD device by detailed comparison to the transport measurements [20, 21, 24, 29].

In this work, we suggest how to extract the entropy of exotic quasiparticles in the multi-channel charge Kondo system from experimental conductance measurements for the above-mentioned device [20, 21]. From the Maxwell relation, the entropy difference between two different gate voltages can be obtained by integration of  $dN/dT$ . While, in principle, one can obtain the entropy change between any two values of gate voltage (see Fig. 1), here we focus on the entropy change occurring as the gate voltage is swept from a state with a unique charge ground state ( $N_g = 0$ ), to a charge degeneracy point ( $N_g = 1/2$ ), which can be written as

$$\Delta S = 2E_C \int_0^{1/2} dN_g \frac{dN}{dT}. \quad (2)$$

For the MCK model, these two points map to a FL ( $N_g = 0$ ), and to a MCK fixed point ( $N_g = 1/2$ ), respectively.

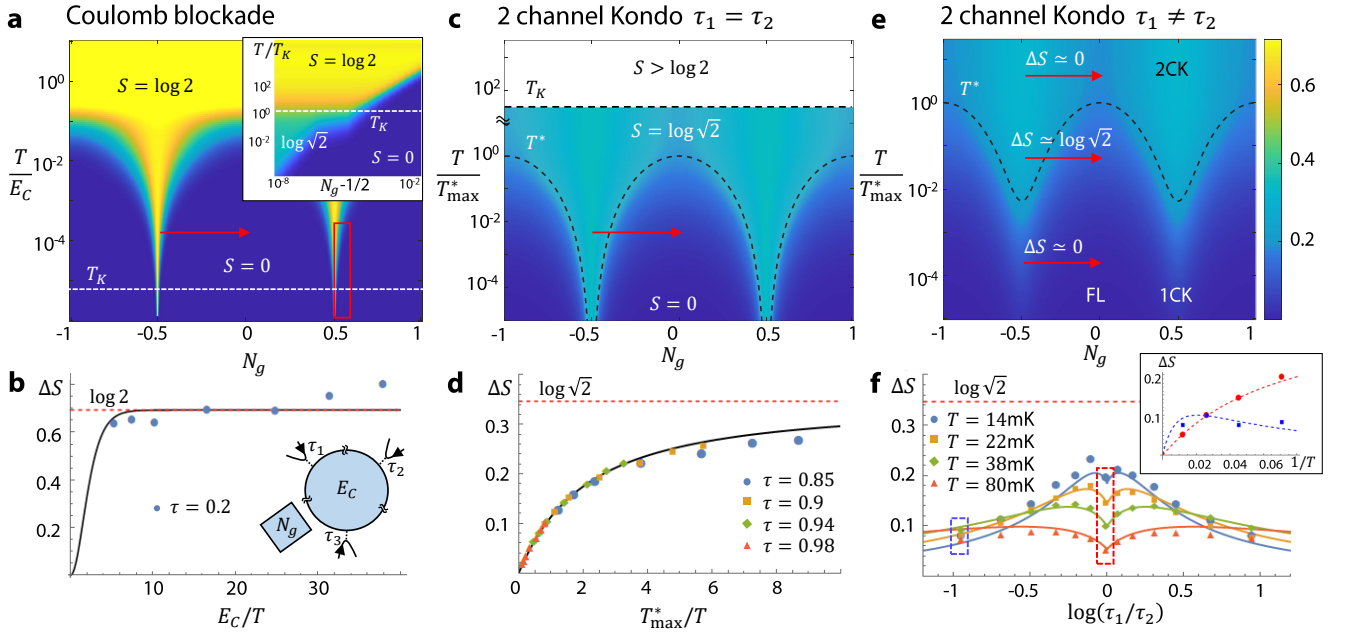


Figure 2. **Extracted entropies for CB and 2CK regimes.** (a) Phase diagram of the charge  $k$ -channel setup - a metallic dot (blue shaded region) coupled to  $k$  leads via quantum point contacts (inset in (b) for  $k = 3$ ) in the Coulomb blockade regime, and for  $k = 2$ :  $T_K$  is much smaller than the experimental temperature. The entropy (in units of the Boltzmann constant) at the degeneracy point ( $N_g = \pm 0.5$ ) is  $\log 2$  while it vanishes in the Coulomb valley, so that the entropy difference, measured along the red arrow, should approach  $\log 2$  at low temperature. The region near charge degeneracy (red box) is equivalent to the two-channel Kondo case, whose phase diagram, obtained from NRG, is shown in the inset. (b) Thermodynamic entropy difference in the CB regime, extracted from the experimental data and Eq. (4). The points correspond to the experimental conductance data for transmission  $\tau = 0.2$  and temperatures  $T = 7.9$  mK, 9.5 mK, 12 mK, 18 mK, 28.9 mK, 40 mK, 55 mK. The solid line corresponds to the theoretical prediction. (c) Phase diagram and impurity entropy of the 2CK regime displaying a crossover between NFL with impurity entropy  $S = \log \sqrt{2}$  and FL with  $S = 0$ . The crossover is governed by the energy scale  $T^*$ , which oscillates with gate voltage. (d) Entropy change extracted from the conductance data and Eq. (2) versus  $T_{\max}^*/T$ . The points correspond to the experimental conductance data for different reflections and different temperatures. Data point corresponds to 7.9mK (55mK) is the rightmost (leftmost) point for each reflection. The solid line corresponds to the theoretical prediction. (e) Phase diagram of the 2CK regime for different values of  $\tau_1$  and  $\tau_2$ . In contrast to the  $\tau_1 = \tau_2$  case, there is a 1CK phase near  $N_g = \pm 0.5$ ,  $T < T^*$ , whose  $S = 0$ . The entropy difference along the red arrows becomes smaller when  $T$  is lower than  $T^*$ . (f) The extracted entropy for different values of  $\tau_1$  and  $\tau_2$ , demonstrating the crossover from the two-channel to the single-channel regimes. When  $\log(\tau_1/\tau_2) < 0$ ,  $\tau_2$  is fixed at 0.93 and  $\tau_1$  varied from 0.36 to 0.93. For  $\log(\tau_1/\tau_2) > 0$ ,  $\tau_1$  is fixed at 0.93 and  $\tau_2$  changes from 0.36 to 0.93. Inset: Temperature dependence of  $\Delta S$  for  $\tau_1 = \tau_2$  (red) and  $\tau_1 \neq \tau_2$  (blue) corresponding to the dashed boxes.

At low temperature, the entropy difference approaches the impurity entropy of the system, or the entropy of the zero mode.

In the rest of the paper we find relations between  $dN/dT$  and the conductance for the different regimes that the charge-Kondo system exhibits corresponding to classical Coulomb blockade (CB), 2CK and 3CK. From these relations, we extract  $dN/dT$  and hence the impurity entropy of the models just from their experimental conductance data. This is subsequently shown to be self-consistent with the thermodynamic impurity entropy directly computed for each model.

First we focus on the CB regime, where the reflections at the QPCs are large enough to satisfy  $E_C \gg T \gg T_K$ . This allows us to exemplify our approach in a relatively simple case. The phase diagram in this regime is depicted in Fig. 2(a), where the red arrow denotes the line along which we calculate the entropy change. The impurity entropy at the degeneracy point ( $N_g = 1/2$ ) is  $S_{\text{imp}} = \log 2$ , signaling two degenerate charge states of the dot, while  $S_{\text{imp}} \simeq 0$  at the Coulomb valley. We extract the entropy difference  $\Delta S$  between  $N_g = 1/2$  and  $N_g = 0$  points from existing conductance data  $G(N_g)$ , by relating the latter to  $dN/dT$ , and then using the Maxwell relation.

In the CB regime, both the conductance and the number of electrons in the dot can be obtained by classical rate

equations. One finds that  $dN_{\text{CB}}/dT$  is proportional to the conductance  $G_{\text{CB}}$ ,

$$\frac{dN_{\text{CB}}}{dT} = \frac{1}{2T} \tanh \frac{E_C(N_g - 1/2)}{T} \frac{G_{\text{CB}}}{G_{\text{CB,max}}}. \quad (3)$$

Here  $G_{\text{CB,max}}$  is the Coulomb peak conductance, which is a function of  $\tau$  and  $T$  [20, 24]. The origin of this relation is that both observables are proportional to the density of states in the dot. Notice that Eq. (3) is not periodic in  $N_g$ , because in assuming  $T \ll E_C$ , we retained only two charge states. Substituting the measured values of the conductance in this formula, we depict in Fig. 2(b)  $\Delta S$  obtained from the experimental conductance. These points can be compared to the theoretical  $\Delta S$ , obtained directly from the thermodynamic free energy (solid line)

$$\Delta S_{\text{CB}} = \log 2 + \frac{E_C/T}{1 + e^{-E_C/T}} - \log(1 + e^{E_C/T}). \quad (4)$$

As  $T \rightarrow 0$ ,  $\Delta S_{\text{CB}} \rightarrow \log 2$ , which corresponds to the two-fold charge degeneracy of the dot. Note that the entropies deduced from the theory and the experimental conductance data do not fully agree. One origin is the large experimental fluctuations of the conductance in the small tunneling regime. Second, there are Kondo corrections due to the 2CK effect (see below) which are not described by the rate equations. These become more important at the lowest temperatures.

Next we focus on the two-channel charge Kondo regime obtained upon tuning two QPCs to be symmetric,  $\tau_1 = \tau_2 \equiv \tau$ , where  $T_K \gg T$  is obtained for large  $\tau$ . Here there is a new energy scale  $T^* = T_{\text{max}}^* \cos^2(\pi N_g)$ , with  $T_{\text{max}}^* = 8\gamma E_C(1 - \tau)/\pi^2$  ( $\gamma = e^{\mathbf{C}}$ ,  $\mathbf{C}$  is the Euler constant). The NFL phase is stabilized for  $T^* \ll T \ll T_K$ , while for  $T < T^*$  the system is in the zero-entropy, FL state (see Fig. 2(c)). Thus, measurement of the entropy change along the solid red line should reveal the entropy change between the FL and NFL states. The model can be mapped to the resonant Majorana tunneling model [14, 24]. The exact solution allows us to obtain the relation

$$\frac{dN_{2\text{CK}}}{dT} = \frac{T_{\text{max}}^* \sin(2\pi N_g)}{4E_C T} \frac{2G_{2\text{CK}}}{G_0}, \quad (5)$$

with  $G_0 = e^2/h$  being the conductance quantum.

Figure 2(d) depicts the deduced entropy, from different sets of conductance measurements, each for a different value of  $\tau$ . The experimental data collapse well onto the scaling form for small reflection, but one can observe small deviations as  $\tau$  is lowered, due to the influence of the leading irrelevant operator [24, 30]. The solid line in the figure is the result of a direct theoretical calculation of the entropy, given by

$$\Delta S_{2\text{CK}} = -\frac{T_{\text{max}}^*}{2\pi T} - \log \left[ \frac{1}{\sqrt{\pi}} \Gamma \left( \frac{1}{2} + \frac{T_{\text{max}}^*}{2\pi T} \right) \right] + \frac{T_{\text{max}}^*}{2\pi T} \Psi \left( \frac{1}{2} + \frac{T_{\text{max}}^*}{2\pi T} \right), \quad (6)$$

where  $\Psi(x)$  is the di-gamma function.

As the temperature becomes lower, the entropy difference  $\Delta S$  approaches  $\log \sqrt{2}$ , the entropy of a single MF. Note that according to the phase diagram depicted in Fig. 2(c), the deviation of experimentally deduced  $\Delta S$  between the FL and NFL regimes from  $\log \sqrt{2}$  is due to the fact that the entropy in the Coulomb valley ( $N_g = 0$ ) does not reach zero. This is because  $T^*$ , which is proportional to  $1 - \tau$ , is necessarily small, and decreasing  $\tau$  will move us away from the 2CK fixed point. Thus at the lowest experimental temperature,  $T = 7.9\text{mK}$ , the entropy difference is about 80% of the expected  $T \rightarrow 0$  value.

Theory predicts that once the transmission coefficients of the two QPCs,  $\tau_1$  and  $\tau_2$ , are not equal, the system will flow from the 2CK fixed point towards one of the 1CK fixed points as temperature decreases (see Fig. 2(e)). Extending the theory to this case, one obtains a relation identical to Eq. (5), except that  $(1 - \tau)$  in the expression for  $T_{\text{max}}^*$  is replaced by  $\sqrt{(1 - \tau_1)(1 - \tau_2)}$ . Applying this relation to the experimental conductance data with different values of  $\tau_1$  and  $\tau_2$ , we obtain  $\Delta S$  along this crossover, showing how the fractional entropy in the NFL phase goes to zero as the channel asymmetry drives the system to the FL, 1CK regime. The experimentally obtained  $\Delta S$  is in quantitative agreement with a direct theoretical calculation of the entropy, shown as solid lines in Fig. 2(f), even beyond the direct applicability regime which requires  $\tau_{1,2} \simeq 1$ . Interestingly,  $\Delta S$  is not a monotonic function of  $\log(\tau_1/\tau_2)$ . This is due to the fact that as one, e.g., decreases  $\tau_2$ ,  $T^*$  increases. As a consequence, the system is first driven closer to the 2CK fixed point, before turning over and flowing toward the 1CK fixed point. Also  $\Delta S$  is not a monotonic function of  $T$  (see the inset of Fig. 2(f)), as illustrated in Fig. 2(e).

We now turn to the 3CK system obtained by tuning  $\tau_1 = \tau_2 = \tau_3 \equiv \tau$ . Here the situation is far more complex, both theoretically and experimentally. From the theory point of view, an analytical solution along the NFL to FL

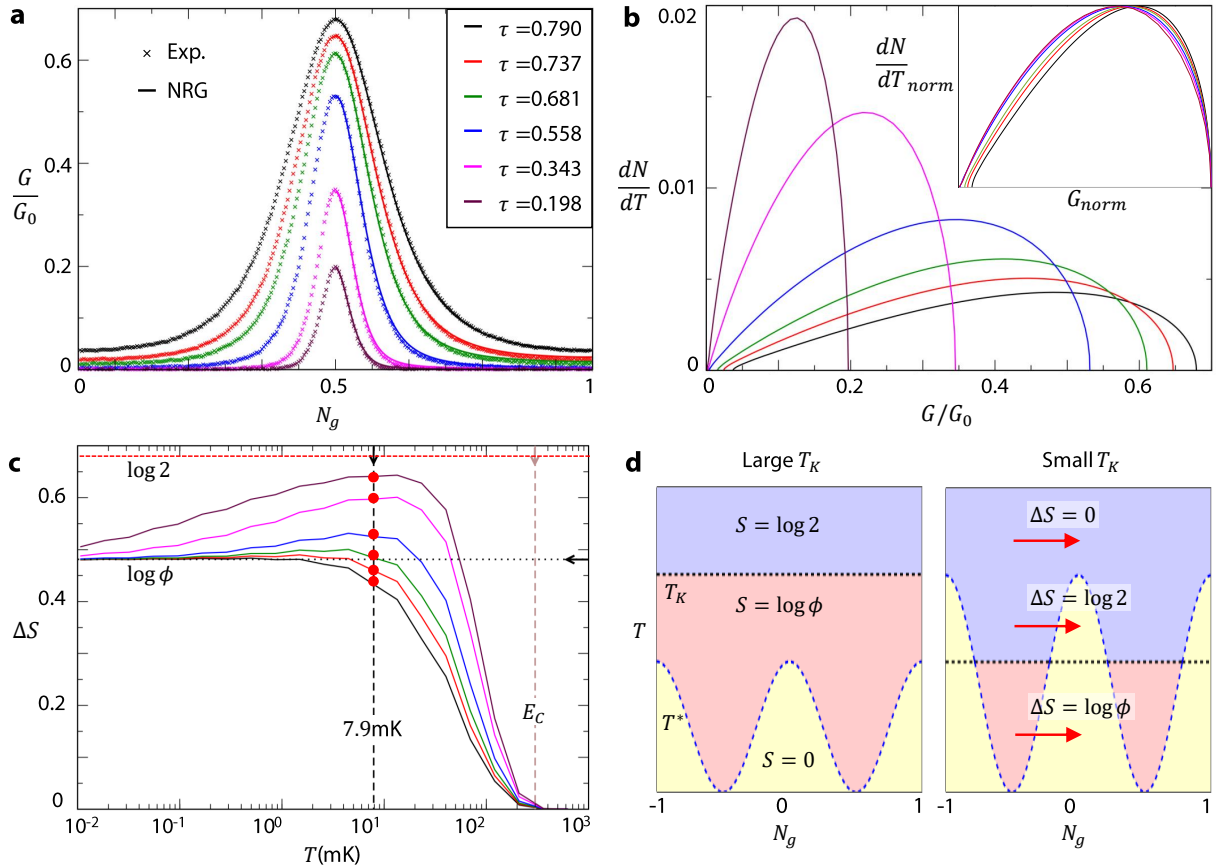


Figure 3. **Entropy for the 3CK regime.** (a) Conductance for the 3CK system as a function of  $N_g$  for different transmissions at  $T = 7.9$  mK, comparing experimental data (points) with NRG calculations (lines). (b) Numerically determined relation between  $dN/dT$  and  $G$  for the same model parameters as in (a). The inset demonstrates the lack of collapse of the normalized quantities, indicating that the experiment is not in the universal regime  $T^* \ll T_K$ . (c) Entropy difference  $\Delta S$  between systems with  $N_g = 0$  and  $\frac{1}{2}$  using the Maxwell relation with the  $dN/dT$ - $G$  relations in panel (d) at  $T = 7.9$  mK (points), compared with  $\Delta S(T)$  obtained by standard thermodynamic NRG calculations for the same systems (lines). (d) Schematic phase diagrams for large transmission (left) and small transmission (right). Blue depicts the CB regime ( $T \gg T_K$ ,  $S = \log(2)$ ), yellow for the FL regime ( $T \ll T^*$ ,  $S = 0$ ), and red for the intermediate NFL regime ( $T^* < T < T_K$ ,  $S = \log \frac{1+\sqrt{5}}{2}$ ). One obtains good scale separation between  $T_K$  and  $T^*$  for all  $N_g$  only at large  $\tau$ .

crossover is not known. So we employ a numerical solution using state-of-the-art numerical renormalization group (NRG) calculations [31–33] to obtain the conductance  $G$  [21] as well as  $dN/dT$  along the crossover. Second, by comparison to the experimental data we note that the experiment is not in the universal regime  $T^* \ll T_K$  (see below). In order to make the comparison with experiment quantitative, we retain multiple dot charge states [28]. Thus, for each experimental conductance curve we obtain the model parameters to best match the conductance lineshapes. We consider a single (base) temperature of  $T = 7.9$  mK and transmissions ranging from  $\tau = 0.79$  to  $\tau = 0.198$  as in the experiment, which corresponds to the crossover regime from  $T \ll T_K$  to  $T \gg T_K$ .

Figure 3(a) depicts the remarkable agreement between the experimental conductance curves and the NRG ones over the entire range of  $N_g$  for all values of the transmission considered. This again validates the theoretical model as an accurate description of the physical device. For these same parameters, NRG also yields  $dN/dT$ , and hence we deduce numerically the relation between  $G$  and  $dN/dT$ , as shown in Fig. 3(b). The inset shows the relation between the normalized  $dN/dT$  and the normalized conductance. Unlike the CB and 2CK cases (Eqs. (3) and (5)), the curves do not collapse onto each other, indicating that the experimental system is not in the universal regime  $T^* \ll T_K$ . Accordingly, for each set of parameters, we use the numerically relation between  $dN/dT$  and  $G$  to determine the entropy difference  $\Delta S$  between gate voltages corresponding to  $N_g = 0$  and  $N_g = 1/2$ . These are marked as circles in Fig. 3(c).

The results are consistent with the entropy obtained from standard thermodynamic NRG calculations (lines), which include the full temperature dependence. For larger transmission we find a direct crossover from  $\Delta S = 0$  to  $\log \phi$ , with

$\phi = \frac{1+\sqrt{5}}{2}$  the golden ratio, for  $T \ll T_K$ , corresponding to the 3CK NFL state hosting a Fibonacci anyon. Interestingly, for small  $\tau$  we find that  $\Delta S$  first approaches  $\log 2$  for  $T \gg T_K$  before approaching  $\log \phi$  at the low-temperature limit. These two behaviours for large and small transmissions are illustrated in the two phase diagrams in Fig. 3(d). For large  $\tau$ , due to large charge fluctuations, the 3CK temperature well exceeds the  $N_g$  dependent crossover scale  $T^*$ . As a result,  $\Delta S$  — which probes gate-voltage sensitivity — increases from 0 to  $\log \phi$  as  $T$  is lowered below the crossover temperature  $T^*$ . For small transmission, however, there are effectively only two charge states as in the familiar spin Kondo problem. Then there is a large gate-voltage sensitivity, which acts as an effective magnetic field on the impurity ‘spin’. Similar to the situation shown in Fig. 2(a), above  $T_K$  the system is described by the CB theory, and below  $T_K$  there is a FL–NFL crossover, leading to the non-monotonic behavior observed in Fig. 3(c) at small  $\tau$ .

To summarize, we described how nontrivial fractional entropy of exotic quasiparticles, such as Majorana fermions and Fibonacci anyons, can be extracted from conductance data. While here we focused on well-characterized charge-Kondo devices, in general, we believe, entropy spectroscopy serves as a smoking-gun probe of exotic anyons in other more controversial systems, including Majorana wires, or other experimental systems realizing Majorana fermions based on the spin Kondo effect [34, 35] or other mechanisms [36].

The general framework is based on thermodynamic Maxwell relations and requires to perform charge measurements as a function of a conjugate chemical potential that causes entropy changes. Here, thanks to a relationship between the charge and the conductance, the self-consistent approach can be already carried out without charge measurements. Our approach opens up a new way to detect nontrivial excitations in quantum impurity systems.

## ACKNOWLEDGMENTS

This project received funding from European Research Council (ERC) under the European Unions Horizon 2020 research and innovation programme under grant agreement No. 951541. AKM acknowledges funding from the Irish Research Council Laureate Awards 2017/2018 through Grant No. IRCLA/2017/169. YM acknowledges support by the Israel Science Foundation (grant 3523/2020). ES acknowledges support from ARO (W911NF-20-1-0013), the Israel Science Foundation grant number 154/19 and US-Israel Binational Science Foundation (Grant No. 2016255).

- 
- [1] Nayak, C., Simon, S. H., Stern, A., Freedman, M. & Sarma, S. D. Non-abelian anyons and topological quantum computation. *Rev. Mod. Phys.* **80**, 1083 (2008).
  - [2] Pan, H. & Sarma, S. D. Physical mechanisms for zero-bias conductance peaks in majorana nanowires. *Phy. Rev. Research* **2**, 013377 (2020).
  - [3] Cooper, N. & Stern, A. Observable bulk signatures of non-abelian quantum hall states. *Phys. Rev. Lett.* **102**, 176807 (2009).
  - [4] Viola, G., Das, S., Grosfeld, E. & Stern, A. Thermoelectric probe for neutral edge modes in the fractional quantum hall regime. *Phys. Rev. Lett.* **109**, 146801 (2012).
  - [5] Ben-Shach, G., Laumann, C. R., Neder, I., Yacoby, A. & Halperin, B. I. Detecting non-abelian anyons by charging spectroscopy. *Phys. Rev. Lett.* **110**, 106805 (2013).
  - [6] Yang, K. & Halperin, B. I. Thermopower as a possible probe of non-abelian quasiparticle statistics in fractional quantum hall liquids. *Phys. Rev. B* **79**, 115317 (2009).
  - [7] Sela, E. *et al.* Detecting the universal fractional entropy of majorana zero modes. *Phys. Rev. Lett.* **123**, 147702 (2019).
  - [8] Hartman, N. *et al.* Direct entropy measurement in a mesoscopic quantum system. *Nat. Phys.* **14**, 1083 (2018).
  - [9] Kleorin, Y. *et al.* How to measure the entropy of a mesoscopic system via thermoelectric transport. *Nat. Commun.* **10** (2019).
  - [10] Nozières, P. & Bladin, A. Kondo effect in real metals. *J. Phys.(Paris)* **41**, 193 (1980).
  - [11] Andrei, N. Diagonalization of the kondo hamiltonian. *Phys. Rev. Lett.* **45**, 379 (1980).
  - [12] Wiegman, P. Exact solution of sd exchange model at T= 0. *JETP Lett* **31**, 364 (1980).
  - [13] Affleck, I. & Ludwig, A. W. Universal noninteger “ground-state degeneracy” in critical quantum systems. *Phys. Rev. Lett.* **67**, 161 (1991).
  - [14] Emery, V. & Kivelson, S. Mapping of the two-channel kondo problem to a resonant-level model. *Phys. Rev. B* **46**, 10812 (1992).
  - [15] Lopes, P. L., Affleck, I. & Sela, E. Anyons in multichannel kondo systems. *Phys. Rev. B* **101**, 085141 (2020).
  - [16] Komijani, Y. Isolating kondo anyons for topological quantum computation. *Phys. Rev. B* **101**, 235131 (2020).
  - [17] Franz, M. Race for majorana fermions. *Physics* **3**, 24 (2010).
  - [18] Leijnse, M. & Flensberg, K. Introduction to topological superconductivity and majorana fermions. *Semiconductor Science and Technology* **27**, 124003 (2012).
  - [19] Beenakker, C. Search for majorana fermions in superconductors. *Annu. Rev. Condens. Matter Phys.* **4**, 113–136 (2013).

- [20] Iftikhar, Z. *et al.* Two-channel kondo effect and renormalization flow with macroscopic quantum charge states. *Nature* **526**, 233 (2015).
- [21] Iftikhar, Z. *et al.* Tunable quantum criticality and super-ballistic transport in a “charge” kondo circuit. *Science* **360**, 5592 (2018).
- [22] Matveev, K. A. Quantum fluctuations of the charge of a metal particle under the coulomb blockade conditions. *Soviet physics, JETP* **72**, 892–899 (1991).
- [23] Matveev, K. A. Coulomb blockade at almost perfect transmission. *Phys. Rev. B* **51**, 1743 (1995).
- [24] Furusaki, A. & Matveev, K. Theory of strong inelastic cotunneling. *Phys. Rev. B* **52**, 16676 (1995).
- [25] Le Hur, K. & Seelig, G. Capacitance of a quantum dot from the channel-anisotropic two-channel kondo model. *Phys. Rev. B* **65**, 165338 (2002).
- [26] Lee, J.-Y. M., Han, C. & Sim, H.-S. Fractional mutual statistics on integer quantum hall edges. *Phys. Rev. Lett.* **125**, 196802 (2020).
- [27] Chamon, C. d. C., Freed, D., Kivelson, S., Sondhi, S. & Wen, X. Two point-contact interferometer for quantum hall systems. *Phys. Rev. B* **55**, 2331 (1997).
- [28] See Supplemental Material for further details.
- [29] Mitchell, A. K., Landau, L., Fritz, L. & Sela, E. Universality and scaling in a charge two-channel kondo device. *Phys. Rev. Lett.* **116**, 157202 (2016).
- [30] Affleck, I. & Ludwig, A. W. Critical theory of overscreened kondo fixed points. *Nucl. Phys. B* **360**, 641–696 (1991).
- [31] Wilson, K. G. The renormalization group: Critical phenomena and the kondo problem. *Rev. Mod. Phys.* **47**, 773 (1975).  
Bulla, R., Costi, T. A. & Pruschke, T. Numerical renormalization group method for quantum impurity systems. *Rev. Mod. Phys.* **80**, 395 (2008).
- [32] Weichselbaum, A. & von Delft, J. Sum-rule conserving spectral functions from the numerical renormalization group. *Phys. Rev. Lett.* **99**, 076402 (2007).
- [33] Mitchell, A. K., Galpin, M. R., Wilson-Fletcher, S., Logan, D. E. & Bulla, R. Generalized wilson chain for solving multichannel quantum impurity problems. *Physical Review B* **89**, 121105 (2014).  
Stadler, K., Mitchell, A., von Delft, J. & Weichselbaum, A. Interleaved numerical renormalization group as an efficient multiband impurity solver. *Phys. Rev. B* **93**, 235101 (2016).
- [34] Potok, R., Rau, I., Shtrikman, H., Oreg, Y. & Goldhaber-Gordon, D. Observation of the two-channel kondo effect. *Nature* **446**, 167 (2007).
- [35] Keller, A. *et al.* Universal fermi liquid crossover and quantum criticality in a mesoscopic system. *Nature* **526**, 237 (2015).
- [36] Mebrahtu, H. *et al.* Observation of majorana quantum critical behaviour in a resonant level coupled to a dissipative environment. *Nat. Phys.* **9**, 732 (2013).
- [37] Glazman, L. & Pustilnik, M. Coulomb blockade and kondo effect in quantum dots. In *New directions in mesoscopic physics (towards nanoscience)*, 93–115 (Springer, 2003).

## METHODS

**Charge-2CK model: bosonization and refermionization.** We start with the original model for the charge Kondo system in Eq. (1). The electron number operator of the QD,  $\hat{N}$ , is defined as

$$\hat{N} = \sum_{j=1}^k \int_0^\infty dx [\psi_{j\text{in}}^\dagger(x) \psi_{j\text{in}}(x) + \psi_{j\text{out}}^\dagger(-x) \psi_{j\text{out}}(-x)]. \quad (7)$$

The range corresponding to the QD is  $0 < x < \infty$  for the incoming modes and from  $-\infty < x < 0$  for the outgoing modes. Using bosonization, the fermion operators are represented by (cf. [24, 25])

$$\psi_{j\nu}^\dagger(x) = \sqrt{\frac{D}{\pi \hbar v_F}} \eta_{j\nu} e^{-i\phi_{j\nu}(x)}. \quad (8)$$

$D$  is bandwidth of the system and  $\eta_{j\nu}$  is a local Majorana fermion ensuring proper anticommutation relations of the various species ( $j = 1, \dots, k; \nu = \text{in, out}$ ) of fermions. Its commutator, satisfying  $\{\eta_{j\nu}, \eta_{j'\nu'}\} = \delta_{j,j'} \delta_{\nu,\nu'}$ . Equivalently there are four boson modes corresponding to the fermion modes, whose commutators are  $[\phi_{j\nu}(x), \phi_{j'\nu'}(y)] = i\pi \text{sgn}(x-y)$  (we use a convention with right-movers only).

We now specify to the 2CK case ( $k = 2$ ). The boson modes are transformed as

$$\begin{pmatrix} \phi_C \\ \phi_I \\ \phi_1 \\ \phi_2 \end{pmatrix} = \frac{1}{2} \begin{pmatrix} 1 & -1 & 1 & -1 \\ 1 & -1 & -1 & 1 \\ 1 & 1 & 1 & 1 \\ 1 & 1 & -1 & -1 \end{pmatrix} \begin{pmatrix} \phi_{1\text{in}} \\ \phi_{1\text{out}} \\ \phi_{2\text{in}} \\ \phi_{2\text{out}} \end{pmatrix}. \quad (9)$$

Also the Majorana fermions are transformed as  $\eta_C \eta_I = \eta_{1\text{in}} \eta_{1\text{out}} = \eta_{2\text{in}} \eta_{2\text{out}}$ . The Hamiltonian becomes

$$\begin{aligned} H_0 &= \sum_{i=1,2,C,I} \int dx \frac{\hbar v_F}{4\pi} (\partial_x \phi_i)^2, \\ H_C &= \frac{E_C}{\pi^2} (\phi_C(0) + \pi N_g)^2, \\ H_B &= \frac{D}{\pi} \eta_C \eta_I (r_1 e^{i\phi_C(0)} + r_2 e^{-i\phi_C(0)}) e^{i\phi_I(0)} + \text{H.C.} \end{aligned} \quad (10)$$

If the charging energy  $E_C$  exceeds all other energy scales, we can integrate out  $\phi_C$  [24, 25]. Subsequently, we have  $e^{i\phi_C(0)} \simeq \sqrt{\frac{2\gamma E_C}{D\pi}} e^{-i\pi N_g}$ . We refermionize the model using  $\psi_I^\dagger(0) = \sqrt{\frac{D}{\pi \hbar v_F}} \eta_I e^{-i\phi_I(0)}$ . For convenience, we denote  $r = \frac{r_1 + r_2}{2}$  and  $\bar{r} = \frac{r_1 - r_2}{2}$ . The Hamiltonian acquires a double-Majorana resonant level form

$$\begin{aligned} H &= \sum_{j=1,2} \frac{\hbar v_F}{4\pi} \int dx (\partial_x \phi_j)^2 + \hbar v_F \int dx \psi_I^\dagger \partial_x \psi_I \\ &+ \sqrt{\frac{8\gamma E_C \hbar v_F}{\pi^2}} (r \cos(\pi N_g) \eta_C (\psi_I(0) - \psi_I^\dagger(0)) + i\bar{r} \sin(\pi N_g) \eta_C (\psi_I(0) + \psi_I^\dagger(0))). \end{aligned} \quad (11)$$

This simple form of the Hamiltonian of the non-trivial 2CK fixed point allows us to obtain analytic expressions for the thermodynamic entropy and for  $dN/dT$ . Their derivation are given in the supplementary information [28].

**$dN/dT$  from conductance: CB and 2CK cases.** In Fig. 4 we compare  $dN/dT$  obtained from experimental conductance data either in the CB or 2CK regimes, using the relations in Eqs. (3), (5), respectively, with the theoretically derived results. In the CB regime, following Ref. [37], we use

$$\frac{dN}{dT} = \frac{1}{2T} \tanh \left[ \frac{E_C(N_g - 1/2)}{T} \right] \frac{2E_C(N_g - 1/2)}{T \sinh(2E_C(N_g - 1/2)/T)}, \quad (12)$$

to draw the solid lines in Fig. 4(a). For the 2CK regime, we use

$$\frac{dN}{dT} = \frac{2\gamma(r^2 - \bar{r}^2)}{\pi^2 T} \sin(2\pi N_g) \left( 1 - \frac{8\gamma E_C}{\pi^2} (r^2 \cos^2(\pi N_g) + \bar{r}^2 \sin^2(\pi N_g)) \psi^{(1)} \left( \frac{1}{2} + \frac{8\gamma E_C}{\pi^2} (r^2 \cos^2(\pi N_g) + \bar{r}^2 \sin^2(\pi N_g)) \right) \right), \quad (13)$$

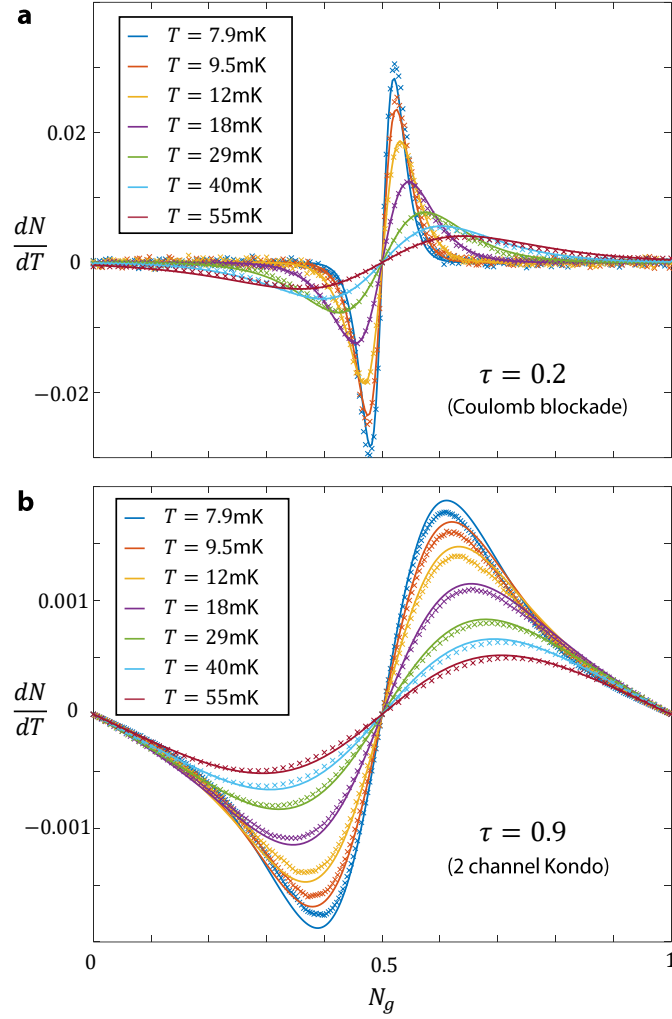


Figure 4. (a)  $dN/dT$  for Coulomb blockade regime ( $\tau = 0.2$ ). Solid lines are theoretical curves (see Supplementary Information) and crossings show the experimentally extracted  $dN/dT$  with Eq. (3). (b)  $dN/dT$  for 2 channel Kondo regime ( $\tau = 0.9$ ). Solid lines are theoretical curves in Eq. (13) and crossings show the experimentally extracted  $dN/dT$  with Eq. (5).

whose derivation is shown in Ref. [28]. For each QPC, the transmission  $0 \leq \tau_i \leq 1$  ( $i = 1, 2, 3$ ) is related to the reflection amplitude  $r_i$  according to [27]  $1 - \tau_i = \frac{r_i^2}{(1+r_i^2/4)^2}$ .

Experimentally extracted values fit with the theory quantitatively well.  $\Delta S$  shown in Fig. 2(b) and (c) is obtained by

$$\Delta S = \frac{1}{2} \left[ - \int_0^{1/2} dN_g \frac{dN}{dT} + \int_{1/2}^1 dN_g \frac{dN}{dT} \right], \quad (14)$$

or averaging over two entropy differences,  $S(N_g = 1/2) - S(N_g = 0)$  and  $S(N_g = 1/2) - S(N_g = 1)$  to reduce experimental error.

**Modeling the charge-3CK model with NRG.** In the original model Eq. (1) the reflections in the QPCs appear as a small perturbation. We apply an alternative description which is equivalent in the large charging energy regime, keeping only a finite number of charge states, and treating the transmission as a perturbation [28, 29].

# Supplementary Information for “Extracting entropy of exotic quasiparticles from conductance measurements”

Cheolhee Han,<sup>1</sup> Andrew K. Mitchell,<sup>2,3</sup> Z. Iftikhar,<sup>4</sup> Yaakov Kleorin,<sup>5</sup> A. Anthore,<sup>4,6</sup> F. Pierre,<sup>4</sup> Yigal Meir,<sup>7</sup> and Eran Sela<sup>1</sup>

<sup>1</sup>*Raymond and Beverly Sackler School of Physics and Astronomy, Tel Aviv University, Tel Aviv 69978, Israel*

<sup>2</sup>*School of Physics, University College Dublin, Belfield, Dublin 4, Ireland*

<sup>3</sup>*Centre for Quantum Engineering, Science, and Technology,  
University College Dublin, Belfield, Dublin 4, Ireland*

<sup>4</sup>*Université Paris-Saclay, CNRS, Centre de Nanosciences et de Nanotechnologies (C2N), 91120 Palaiseau, France*

<sup>5</sup>*Center for the Physics of Evolving Systems, University of Chicago, Chicago, IL, 60637, USA*

<sup>6</sup>*Université de Paris, C2N, 91120 Palaiseau, France*

<sup>7</sup>*Department of Physics, Ben-Gurion University of the Negev, Beer-Sheva, 84105 Israel*

(Dated: August 31, 2021)

## I. SUPPLEMENTARY NOTE: DERIVATION OF EQ. (5)

In this supplementary note, we calculate the expectation value of the number of electrons in the quantum dot for the 2CK model. We start by writing the Hamiltonian in Eq. (11) in a simpler form. We first rotate the fermion modes as

$$\begin{aligned}\chi_I &= \frac{1}{i\sqrt{2}} \frac{1 + i\frac{\bar{r}}{r} \tan(\pi N_g)}{\sqrt{1 + \frac{\bar{r}^2}{r^2} \tan^2(\pi N_g)}} \psi_I - \frac{1}{i\sqrt{2}} \frac{1 - i\frac{\bar{r}}{r} \tan(\pi N_g)}{\sqrt{1 + \frac{\bar{r}^2}{r^2} \tan^2(\pi N_g)}} \psi_I^\dagger, \\ \bar{\chi}_I &= \frac{1}{\sqrt{2}} \frac{1 + i\frac{\bar{r}}{r} \tan(\pi N_g)}{\sqrt{1 + \frac{\bar{r}^2}{r^2} \tan^2(\pi N_g)}} \psi_I + \frac{1}{\sqrt{2}} \frac{1 - i\frac{\bar{r}}{r} \tan(\pi N_g)}{\sqrt{1 + \frac{\bar{r}^2}{r^2} \tan^2(\pi N_g)}} \psi_I^\dagger.\end{aligned}\tag{S1}$$

Using this notation, the Hamiltonian becomes

$$\begin{aligned}H &= \sum_{\nu=1,2} \frac{\hbar v_F}{4\pi} \int dx (\partial_x \phi_\nu)^2 + i\hbar v_F \int dx \bar{\chi}_I \partial_x \bar{\chi}_I + i\hbar v_F \int dx \chi_I \partial_x \chi_I \\ &\quad + i4 \sqrt{\frac{\gamma E_C \hbar v_F}{\pi^2} [r^2 \cos^2(\pi N_g) + \bar{r}^2 \sin^2(\pi N_g)]} \eta_C \chi_I(0).\end{aligned}\tag{S2}$$

From this model we can obtain the thermodynamic entropy as [1, 2],

$$S = \int_{-E_C}^{E_C} \frac{d\omega}{2\pi} \frac{\frac{8\gamma E_C \hbar v_F}{\pi^2} (r^2 \cos^2(\pi N_g) + \bar{r}^2 \sin^2(\pi N_g))}{\omega^2 + [\frac{8\gamma E_C \hbar v_F}{\pi^2} (r^2 \cos^2(\pi N_g) + \bar{r}^2 \sin^2(\pi N_g))]^2} \left[ \frac{\omega/T}{1 + e^{\omega/T}} + \log(1 + e^{-\omega/T}) \right].\tag{S3}$$

Equation (S3) is used to draw Fig. 2(c) and (e). For Fig. 2(c) we use  $r = 0.3987$ , and for Fig. 2(e) we use  $r = 0.3962$  and  $\bar{r} = 0.1269$ .

The average electron's number of the dot can be obtained using the relation

$$N = N_g - \frac{1}{2E_C} \frac{\partial F}{\partial N_g}.\tag{S4}$$

After computing  $\partial_{N_g} F$ , the charge deviation becomes

$$N = N_g - \sqrt{\frac{2\gamma \hbar v_F}{E_C}} \int_{-E_C}^{E_C} \frac{d\omega}{2\pi} \left[ -r \sin(\pi N_g) \langle \eta_C (\psi_I(0) - \psi_I^\dagger(0)) \rangle(\omega) + i\bar{r} \cos(\pi N_g) \langle \eta_C (\psi_I(0) + \psi_I^\dagger(0)) \rangle(\omega) \right].\tag{S5}$$

The energy integration is bounded by  $E_C$ , which is a high energy cutoff appearing after integrating out  $\phi_C$ . We can compute the correlators  $\langle \eta_C \psi_I(0) \rangle$  or  $\langle \eta_C \psi_I^\dagger(0) \rangle$  by changing the basis back as in Eq. (S1).

Combining Eqs. (S4) and (S1), the number expectation value becomes

$$N = N_g + 2(r^2 - \bar{r}^2) \sqrt{\frac{\gamma \hbar v_F}{E_C}} \sin(\pi N_g) \cos(\pi N_g) \frac{1}{\sqrt{r^2 \cos^2(\pi N_g) + \bar{r}^2 \sin^2(\pi N_g)}} \int_{-E_C}^{E_C} \frac{d\omega}{2\pi} (-i) \langle \eta_C \chi_I(0) \rangle.\tag{S6}$$

Then  $dN/dT$  becomes

$$\frac{dN}{dT} = 2(r^2 - \bar{r}^2) \sqrt{\frac{\gamma \hbar v_F}{E_C}} \sin(\pi N_g) \cos(\pi N_g) \frac{1}{\sqrt{r^2 \cos^2(\pi N_g) + \bar{r}^2 \sin^2(\pi N_g)}} \partial_T \int \frac{d\omega}{2\pi} (-i) \langle \eta_C \chi_I(0) \rangle.$$

Next we calculate the conductance. The current operator is

$$\begin{aligned} I &= e \partial_t \frac{1}{2} \left( \int_{-\infty}^0 dx (\psi_{1\text{in}}^\dagger \psi_{1\text{in}} - \psi_{2\text{in}}^\dagger \psi_{2\text{in}}) + \int_0^\infty dx (\psi_{1\text{out}}^\dagger \psi_{1\text{out}} - \psi_{2\text{out}}^\dagger \psi_{2\text{out}}) \right) \\ &= \frac{e}{2\pi} \partial_t \phi_I(0) = e \bar{\chi}_I(0) \chi_I(0). \end{aligned} \quad (\text{S7})$$

The conductance is

$$\begin{aligned} G &= \frac{i}{2\hbar} \int dt t \langle [I(t), I(0)] \rangle = -\frac{e^2}{2\hbar} \int \frac{d\omega}{2\pi} A(\chi_I(0), \chi_I(0); \omega) A(\bar{\chi}_I(0), \bar{\chi}_I(0); -\omega) \partial_\omega n_F(\omega/T) \\ &= -\frac{e^2}{2\hbar} \int \frac{d\omega}{2\pi} A(\chi_I(0), \chi_I(0); \omega) \partial_\omega n_F(\omega/T) = \frac{e^2}{2\hbar} \int \frac{d\omega}{2\pi} A(\chi_I(0), \chi_I(0); \omega) \frac{T}{\omega} \partial_T n_F(\omega/T) \\ &= \frac{e^2}{2\hbar} T \partial_T \int \frac{d\omega}{2\pi \omega} \langle \chi_I(0) \chi_I(0) \rangle(\omega) \\ &= \frac{e^2}{2\hbar} T \frac{1}{\sqrt{\frac{16\gamma E_C}{\hbar v_F \pi^2} [r^2 \cos^2(\pi N_g) + \bar{r}^2 \sin^2(\pi N_g)]}} \partial_T \int \frac{d\omega}{2\pi} (-i) \langle \eta_C \chi_I(0) \rangle(\omega). \end{aligned} \quad (\text{S8})$$

Here  $A(\chi_I(0), \chi_I(0); \omega)$  is spectral function of operator  $\chi_I(0)$  at energy  $\omega$ . In the calculation, we use  $A(\bar{\chi}_I(0), \bar{\chi}_I(0); \omega) = 1$  for non-interacting  $\bar{\chi}_I$ , and the equation of motion of  $\chi_I$ ,

$$\sqrt{\frac{16\gamma E_C}{\hbar v_F \pi^2} [r^2 \cos^2(\pi N_g) + \bar{r}^2 \sin^2(\pi N_g)]} \chi_I(0, \omega) = -i\omega \eta_C(\omega). \quad (\text{S9})$$

Then

$$\frac{dN}{dT} = \frac{2\gamma}{\pi^2 T} (r^2 - \bar{r}^2) \sin(2\pi N_g) \frac{2G}{G_0}, \quad (\text{S10})$$

where again  $G_0 = e^2/h$ .

Now we obtain the expressions for  $dN/dT$  and  $G$ . From the correlators

$$\begin{aligned} \langle \eta_C \chi_I(0) \rangle(\omega) &= \frac{i\omega \sqrt{\frac{16\gamma E_C}{\hbar v_F \pi^2} [r^2 \cos^2(\pi N_g) + \bar{r}^2 \sin^2(\pi N_g)]}}{\omega^2 + \left[ \frac{8\gamma E_C}{\pi^2} [r^2 \cos^2(\pi N_g) + \bar{r}^2 \sin^2(\pi N_g)] \right]^2} \frac{1}{1 + e^{-\omega/T}}, \\ \langle \eta_C \bar{\chi}_I(0) \rangle(\omega) &= 0, \end{aligned} \quad (\text{S11})$$

we can integrate Eq. (S7) and Eq. (S8), leading to

$$\frac{dN}{dT} = \frac{2\gamma(r^2 - \bar{r}^2)}{\pi^2 T} \sin(2\pi N_g) \left( 1 - \frac{\frac{8\gamma E_C}{\pi^2} (r^2 \cos^2(\pi N_g) + \bar{r}^2 \sin^2(\pi N_g))}{2\pi T} \psi^{(1)} \left( \frac{1}{2} + \frac{\frac{8\gamma E_C}{\pi^2} (r^2 \cos^2(\pi N_g) + \bar{r}^2 \sin^2(\pi N_g))}{2\pi T} \right) \right), \quad (\text{S12})$$

and

$$G = \frac{G_0}{2} \left( 1 - \frac{\frac{8\gamma E_C}{\pi^2} (r^2 \cos^2(\pi N_g) + \bar{r}^2 \sin^2(\pi N_g))}{2\pi T} \psi^{(1)} \left( \frac{1}{2} + \frac{\frac{8\gamma E_C}{\pi^2} (r^2 \cos^2(\pi N_g) + \bar{r}^2 \sin^2(\pi N_g))}{2\pi T} \right) \right). \quad (\text{S13})$$

Equation (5) of the main text relating  $dN/dT$  with  $G$  follows from Eqs. (S12) and (S13).

The extracted entropy  $\Delta S$  is obtained as

$$\Delta S = -\frac{4\gamma E_C}{\pi^3 T} (r^2 - \bar{r}^2) + \log \left[ \frac{\Gamma(\frac{1}{2} + \frac{4\gamma E_C \bar{r}^2}{\pi^3 T})}{\Gamma(\frac{1}{2} + \frac{4\gamma E_C r^2}{\pi^3 T})} \right] + \frac{4\gamma E_C}{\pi^3 T} \left[ r^2 \psi^{(0)} \left( \frac{1}{2} + \frac{4\gamma E_C r^2}{\pi^3 T} \right) - \bar{r}^2 \psi^{(0)} \left( \frac{1}{2} + \frac{4\gamma E_C \bar{r}^2}{\pi^3 T} \right) \right]. \quad (\text{S14})$$

It is used to draw solid lines in Fig. 2(d) and (f).

## II. SUPPLEMENTARY NOTE: LEADING IRRELEVANT CORRECTION TO EQ. (5)

In this supplementary note, we calculate the leading irrelevant corrections to  $dN/dT$  and  $G$ . The lowest order corrections are

$$\delta \left( \frac{dN}{dT} \right) = \frac{2r^2\gamma}{\pi^2} \sin(2\pi N_g) \frac{\pi^4 T}{4E_C^2} \left[ \frac{1}{12} + 2 \log \left( \frac{2E_C}{\pi T} \right) \right], \quad (\text{S15})$$

$$\delta G = -\frac{G_0}{2} \frac{\pi^3 \gamma T}{16E_C} r^2 \sin^2(\pi N_g). \quad (\text{S16})$$

Equation (S16) is derived in Ref. [3]. Below we will derive Eq. (S15). By inspection, we see that these corrections violate the relation in Eq. (5). Therefore Eq. (5) holds only for small  $r$ , small  $T$ , and large  $E_C$ .

To compute the leading irrelevant correction to  $dN/dT$ , we use the bosonized description and treat the reflection as a perturbation. The leading irrelevant contribution to the conductance is computed within this framework in Ref. [3].

The Lagrangian of the system is  $\mathcal{L} = \mathcal{L}_0 + \mathcal{L}_C + \mathcal{L}_B$  where

$$\begin{aligned} \mathcal{L}_0 &= \sum_{i=1,2,I,C} \frac{\hbar v_F}{4\pi} \int dx \partial_x \phi_i (\partial_t \phi_i - \partial_x \phi_i), \\ \mathcal{L}_C &= -\frac{E_C}{\pi^2} (\phi_C(0) + \pi N_g)^2, \\ \mathcal{L}_B &= -\frac{Dr}{\pi} e^{i(\phi_I(0) + \phi_C(0))} + e^{i(\phi_I(0) - \phi_C(0))} + \text{H.C.} \end{aligned} \quad (\text{S17})$$

We Fourier transform the boson fields as

$$\phi_i(x, \tau) = \sqrt{\frac{T}{L}} \sum_{\omega_n, q} \phi_i(q, \omega_n) e^{iqx - i\omega_n \tau}, \quad (\text{S18})$$

where  $\omega_n = 2\pi T n / \hbar$ ,  $L$  is system size, and  $\tau$  is imaginary time. The bare action is transformed to

$$\mathcal{S}_0 = - \sum_{\omega_n, q} -\frac{q(q - i\omega_n)}{4\pi} \phi_C(q, \omega_n) \phi_C(-q, -\omega_n). \quad (\text{S19})$$

We now focus on the  $\phi_C$  and  $\phi_I$  fields. Heading towards a perturbative expansion in the backscattering term  $\mathcal{L}_B$ , we integrate these two fields away from  $x = 0$ . Neglecting  $\mathcal{L}_B$  at first, and noticing that the fields  $\phi_{1,2}$  are decoupled, we obtain

$$\begin{aligned} \mathcal{Z}_{\phi_I} &= \int \mathcal{D}\phi_I \exp \left[ - \sum_{\omega_n} \frac{|\omega_n|}{2\pi} \phi_I(\omega_n) \phi_I(-\omega_n) \right], \\ \mathcal{Z}_{\phi_C} &= \int \mathcal{D}\phi_C \exp \left[ - \sum_{\omega_n} \left( \left[ \frac{|\omega_n|}{2\pi} + \frac{E_C}{\pi^2} \right] \phi_C(\omega_n) \phi_C(-\omega_n) \right) + \frac{2E_C}{\pi} \frac{1}{\sqrt{T}} N_g \phi_C(\omega_n = 0) - \frac{E_C}{T} N_g^2 \right]. \end{aligned} \quad (\text{S20})$$

Now we expand the perturbation  $\mathcal{L}_B$ . Then the partition function can be expanded as  $\mathcal{Z} \simeq \mathcal{Z}_1 + \frac{D^2 r^2}{2\pi^2} \mathcal{Z}_2$ , where  $\mathcal{Z}_1 = \mathcal{Z}_{\phi_I} \mathcal{Z}_{\phi_C}$ , and  $\mathcal{Z}_2$  is written as

$$\begin{aligned} \mathcal{Z}_2 &= \sum_{\xi_1 \xi_2 = \pm 1} \int_0^{\frac{\hbar}{T}} d\tau_1 d\tau_2 \int \mathcal{D}\phi_I \mathcal{D}\phi_C \exp \left[ - \sum_{\omega_n} \left( \frac{|\omega_n|}{2\pi} \phi_I(\omega_n) \phi_I(-\omega_n) - i\sqrt{T} \xi_1 (e^{-i\omega_n \tau_1} - e^{-i\omega_n \tau_2}) \phi_I(\omega_n) \right) \right] \\ &\times \exp \left[ - \sum_{\omega_n} \left( \left[ \frac{|\omega_n|}{2\pi} + \frac{E_C}{\pi^2} \right] \phi_C(\omega_n) \phi_C(-\omega_n) - i\sqrt{\frac{T}{\hbar}} \xi_1 (e^{-i\omega_n \tau_1} - \xi_2 e^{-i\omega_n \tau_2}) \phi_C(\omega_n) \right) + \frac{2E_C N_g}{\pi \sqrt{T/\hbar}} \phi_C(\omega_n = 0) - \frac{E_C}{T} N_g^2 \right]. \end{aligned}$$

Here  $\xi_1, \xi_2 = \pm 1$  indicate the tunneling directions ( $\xi_1$ ) and tunneling positions ( $\xi_2$ ). From Eq. (S4), the electron's number in the quantum dot is

$$N = N_g - \frac{T}{2E_C} \frac{1}{\mathcal{Z}} \frac{d\mathcal{Z}}{dN_g} \simeq N_g - \frac{2r^2\gamma}{\pi^2} \sin(2\pi N_g) \frac{T}{\hbar} \int_0^{\frac{\hbar}{T}} d\tau_1 \int_0^{\frac{\hbar}{T}} d\tau_2 \frac{\pi T}{\sin(\frac{\pi T}{\hbar} |\tau_1 - \tau_2|)} \left[ 1 - \frac{\pi^4 T^2}{4E_C^2 \sin^2(\frac{\pi T}{\hbar} (\tau_1 - \tau_2))} \right]. \quad (\text{S21})$$

To integrate Eq. (S21), we introduce the infinitesimal time  $\tau_0$ , which corresponds to the inverse of the bandwidth (or  $\hbar/E_C$ ),

$$\int_0^{\hbar/T} d\tau \frac{\pi T}{\sin(\pi T \tau / \hbar)} = \int_{\tau_0}^{\hbar/T - \tau_0} d\tau \frac{\pi T}{\sin(\pi T \tau / \hbar)} = 2\hbar \log\left(\frac{2}{\tau_0 \pi T}\right), \quad (\text{S22})$$

$$\int_0^{\hbar/T} d\tau \frac{(\pi T)^3}{\sin(\pi T \tau / \hbar)^3} = \int_{\tau_0}^{\hbar/T - \tau_0} d\tau \frac{(\pi T)^3}{\sin(\pi T \tau / \hbar)^3} = \hbar^3 \left[ \tau_0^2 T^2 - \frac{\pi^2}{6} + \pi^2 \log\left(\frac{2\hbar}{\pi \tau_0 T}\right) \right]. \quad (\text{S23})$$

After integrating  $\tau_1$  and  $\tau_2$  we have

$$N \simeq N_g - 2 \sin(2\pi N_g) \frac{r^2}{\pi^2} \gamma \log\left(\frac{2E_C}{\pi T}\right) - 2 \sin(2\pi N_g) \gamma r^2 \left[ \frac{1}{8} - \frac{\pi^2 T^2}{6E_C^2} + \frac{\pi^2 T^2}{4E_C^2} \log\left(\frac{2E_C}{\pi T}\right) \right], \quad (\text{S24})$$

and  $dN/dT$  becomes

$$\frac{dN}{dT} \simeq \frac{2r^2\gamma}{\pi^2} \sin(2\pi N_g) \frac{1}{T} + \frac{2r^2\gamma}{\pi^2} \sin(2\pi N_g) \frac{\pi^4 T}{4E_C^2} \left[ \frac{1}{12} + 2 \log\left(\frac{2E_C}{\pi T}\right) \right]. \quad (\text{S25})$$

The first term corresponds to a Taylor expansion for small  $r$  of our result in Eq. (S12) (with  $\bar{r} = 0$ ). The second part corresponds to the leading irrelevant corrections in Eq. (S15).

### III. SUPPLEMENTARY NOTE : DETAILS OF NRG CALCULATIONS

To simulate the experimental 3CCK system using NRG, we implement a generalization of the standard 3CK model to include multiple dot charging states and a finite charging energy  $E_C$ . Following Matveev [3] we identify three distinct channels of conduction electrons  $\alpha = 1, 2, 3$  around each of the three QPCs connecting the dot to the leads. We label electrons on the physical leads as  $\sigma = \uparrow$  and electrons on the dot as  $\sigma = \downarrow$  (even though in reality the electrons are effectively spinless due to the large applied magnetic field). Without interactions, the three channels are to a good approximation independent because of the decohering Ohmic contact [4], which gives a long dwell time for electrons on the dot. However, tunneling events at the QPCs become correlated due to the dot charging energy  $E_C$ . Tunneling of electrons onto or off the dot changes the number of dot electrons  $N$ , and hence its electrostatic energy due to the Coulomb interaction. A gate voltage  $V_g$  is used to tune the average dot filling, and hence  $N_g$ .

The Hamiltonian reads,  $H_{3\text{CCK}} = \sum_{\alpha} (H_{\text{leads}}^{\alpha} + H_{\text{dot-lead}}^{\alpha}) + H_{\text{int}} + H_{\text{gate}}$ . Here,

$$H_{\text{leads}}^{\alpha} = \sum_{k,\sigma} \epsilon_k c_{\alpha k \sigma}^{\dagger} c_{\alpha k \sigma}, \quad (\text{S26})$$

describes each effective spinfull conduction electron channel. For simplicity, we take equivalent leads with a constant density of states  $\nu = 1/2D$  inside a band of half-width  $D$ .

Electronic tunneling between the dot and lead  $\alpha$  is described by,

$$H_{\text{dot-lead}}^{\alpha} = J_{\alpha} (c_{\alpha \downarrow}^{\dagger} c_{\alpha \uparrow} \hat{S}^+ + c_{\alpha \uparrow}^{\dagger} c_{\alpha \downarrow} \hat{S}^-), \quad (\text{S27})$$

where  $c_{\alpha \sigma} = \sum_k a_k c_{\alpha k \sigma}$  is a localized lead orbital at the dot position. We define  $\hat{S}^+ = \sum_{N_d=N_0-\bar{N}}^{N_0+\bar{N}-1} |N_d+1\rangle \langle N_d|$  as an operator that increases the number of dot electrons by one unit (and correspondingly  $\hat{S}^- = (\hat{S}^+)^{\dagger}$  decreases the dot charge), which thereby keeps track of the electron localization in either lead or dot around each QPC. Here  $N_0$  is some fixed reference number of electrons, while  $\bar{N}$  determines the number of accessible dot charge states. Formally  $N_0, \bar{N} \rightarrow \infty$ , however in practice a finite number of charge states  $\bar{N}$  can be retained in the NRG calculations, provided the QPC transmission is not too high, and the temperature is low enough compared with the charging energy  $E_C$ . One can check *post hoc* that the results of NRG calculations are converged with respect to increasing  $\bar{N}$  for a given set of physical model parameters.

Electron interactions on the dot are embodied by the charging term,

$$H_{\text{int}} = E_C (\hat{N}_d - N_0)^2, \quad (\text{S28})$$

with  $\hat{N}_d = \sum_{\alpha,k} c_{\alpha k \downarrow}^{\dagger} c_{\alpha k \downarrow}$  the total dot number operator such that  $\hat{N}_d |N_d\rangle = N_d |N_d\rangle$ . With the gate voltage term  $H_{\text{gate}} = -eV_g \hat{N}_d$ , we may write  $H_{\text{int}} + H_{\text{gate}} = E_C (\hat{N}_d - N_0 - N_g)^2$  up to an irrelevant overall constant, with

$eV_g = 2E_C N_g$ . In the following we refer only to  $N_g$ , but it should be understood that this is tunable in practice through  $V_g$ .

Note that for half-integer  $N_0$  and  $E_C \rightarrow \infty$ , only the lowest two dot charge states survive, and the model becomes equivalent to a spin-anisotropic version of the standard spin-3CK model. However, in this work, we use a finite value of  $E_C$  and retain multiple charge states. Specifically, we take  $E_C = 300\text{mK}$  and  $T = 7.9\text{mK}$  as in the experiment, and set  $D/E_C = 10$ . We choose  $N_0$  to be half-integer and take  $\bar{N} = 5$ , meaning that in total 10 dot charge states are retained in the NRG calculations. We have confirmed that the results are insensitive to further increasing  $D/E_C$  and  $\bar{N}$ . We focus on the properties at the critical point, for which we have equal couplings,  $J_\alpha \equiv J$ .

The above model is solved using Wilson's NRG method [5], which involves the logarithmic discretization of the conduction electron bands, mapping them to Wilson chains, and then iteratively diagonalizing the discretized model. Retaining only  $N_s$  of the lowest energy states at each step amounts to an RG procedure in which the physics on progressively lower energy scales is revealed.

However, standard NRG cannot be used here due to the complexity of the model at hand (in particular its three conduction channels). Instead, we use the 'interleaved NRG' (iNRG) method [6], which involves mapping all three channels to a single generalized Wilson chain. This dramatically lowers the computational cost of such calculations, and brings the numerical solution of the 3CCK model within reach. We exploit conserved charge in each channel and conserved total spin, use a discretization parameter  $\Lambda = 3$  and keep  $N_s = 60000$  states at each step of the calculation.

To compare with experiment, we calculate the dc linear response differential conductance,

$$G_{\alpha\beta} = \left. \frac{dI^\alpha}{dV_b^\beta} \right|_{V_b^\beta \rightarrow 0} \quad (\text{S29})$$

where  $I^\alpha = -e\langle\dot{N}_{\alpha\uparrow}\rangle$  is the current into lead  $\alpha$  and  $V_b^\beta$  is the voltage bias applied to lead  $\beta$ . Here  $\dot{N}_{\alpha\uparrow} = \frac{d}{dt}\hat{N}_{\alpha\uparrow}$  and  $\hat{N}_{\alpha\uparrow} = \sum_k c_{\alpha k\uparrow}^\dagger c_{\alpha k\uparrow}$ . An ac voltage bias on lead  $\beta$  can be incorporated by a source term in the Hamiltonian,  $H_{\text{bias}}^\beta = -eV_b^\beta \cos(\omega t)\hat{N}_{\beta\uparrow}$ , where  $\omega$  is the ac driving frequency. The dc limit is obtained as  $\omega \rightarrow 0$ .

The geometry of the charge Kondo device means that conductance cannot be related simply to a dot spectral function, and we must use the Kubo formula instead,

$$G_{\alpha\beta}/G_0 = \lim_{\omega \rightarrow 0} \frac{-2\pi \text{Im}K_{\alpha\beta}(\omega)}{\omega}, \quad (\text{S30})$$

where  $G_0 = e^2/h$  as before, and  $K_{\alpha\beta}(\omega) = \langle\langle\dot{N}_{\alpha\uparrow}; \dot{N}_{\beta\uparrow}\rangle\rangle$  is the Fourier transform of the retarded current-current correlator  $K_{\alpha\beta}(t) = -i\theta(t)\langle[\dot{N}_{\alpha\uparrow}, \dot{N}_{\beta\uparrow}(t)]\rangle$ . Within iNRG,  $\text{Im}K_{\alpha\beta}(\omega)$  may be obtained from its Lehmann representation using the full density matrix technique [7]. In fact, the numerical evaluation is substantially improved by utilizing the identity  $\text{Im}K_{\alpha\beta}(\omega) = -\omega^2 \text{Im}\langle\langle\hat{N}_{\alpha\uparrow}; \hat{N}_{\beta\uparrow}\rangle\rangle$  [8]. Due to the channel symmetry considered here,  $G_{\alpha\neq\beta} = -2G_{\alpha\alpha} \equiv G$ .

Next, we fine-tuned the model couplings  $J$  so as to fit the NRG conductance lineshapes for the Coulomb peak, obtained by varying  $N_g$ , to the corresponding experimental data at a given transmission  $\tau$ . Remarkable agreement is obtained over the entire range of  $N_g$  for each  $\tau$  considered, as shown in Fig. 3(b). The fitted model  $J$  for each experimental  $\tau$  is given in Table I.

Experimental transmission, $\tau$	0.790	0.737	0.681	0.558	0.343	0.198
NRG coupling, $J/D$	0.41	0.39	0.37	0.34	0.27	0.22
NRG effective transmission, $\tau_{\text{eff}}$	0.83	0.79	0.75	0.68	0.51	0.37

Table I. Optimized NRG couplings use to fit calculated conductance lineshapes to experimental data in Fig. 3(b).

The effective QCP transmission  $\tau_{\text{eff}}$  can be estimated from the low-temperature conductance of a tunnel junction between two non-interacting leads, where the tunneling matrix element is  $J$  and all other interactions are ignored. This yields the standard result,

$$\tau_{\text{eff}} = \frac{4(\pi\nu J)^2}{[1 + (\pi\nu J)^2]^2}, \quad (\text{S31})$$

also given for comparison in Table I. Although a good rule of thumb, it is evident that quantitative simulation requires a more sophisticated fitting procedure than simply using  $\tau_{\text{eff}}$ .

Importantly, for  $\tau = 0.79$  and low temperatures  $T = 7.9\text{mK}$ , the conductance approaches closely the nontrivial 3CCK fixed point value of  $G/G_0 = 2\sin^2(\pi/5)$ , as also captured by NRG. We note however that at large transmissions

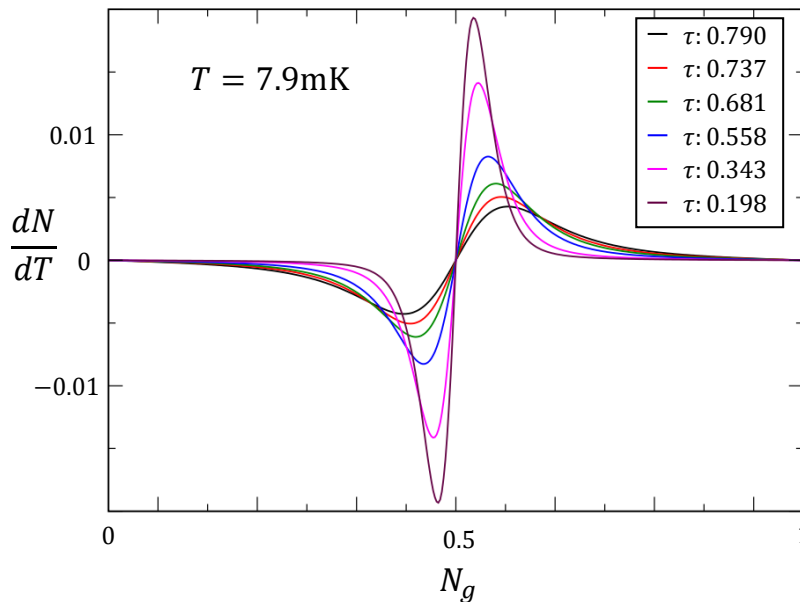


Figure S1.  $dN/dT$  vs  $N_g$  for the 3CCK model with different transmissions at  $T = 7.9\text{mK}$ . Parameters tuned as in Fig. 3 to match the experimental conductance lineshapes (See Table I). Here we measure energy in units of mK.

$\tau \sim 0.79$ , the Kondo temperature  $T_K$  found in the experiment diverges [4], indicating that a macroscopic number of dot charge states are involved in the screening process. This effect cannot be captured with NRG, which necessitates using a relatively small finite  $\bar{N}$  (the maximum  $T_K$  in NRG is around  $E_C$ ). This means that the comparison between experiment and theory at high transmission breaks down at elevated temperatures. We therefore confine our discussion here to the experimental base temperature  $T = 7.9\text{mK}$  ( $\ll E_C$ ) which still affords a good comparison at large  $\tau$  (and noting that such issues do not arise at smaller  $\tau$  since then  $T_K \ll E_C$  anyway).

Finally, we comment on the static thermodynamic quantity  $N = \langle \hat{N}_d \rangle - N_0$ , which can be calculated at any temperature  $T$  within NRG. For the same set of parameters as used for Fig. 3(b), we obtain  $N$  as a function of gate voltage, over the Coulomb oscillation period  $0 \leq N_g \leq 1$  at temperatures  $T = 7.9\text{mK}$  and  $T' = 7.901\text{mK}$ . Although  $\Delta N = N(T) - N(T')$  is very small for this  $\Delta T = 0.001\text{mK}$  temperature difference, the NRG calculations are highly accurate and allow for an excellent finite-difference approximation to the derivative  $dN/dT \simeq \Delta N/\Delta T$  (the exact derivative can also be obtained by differentiable programming techniques [9]). The results are presented in Fig. S1.

Note in particular that the full model has exact particle-hole symmetry at all integer and half-integer values of  $N_g$ . This means that  $N$  is a constant and independent of temperature at these points. This is reflected in Fig. S1 by the condition  $dN/dT = 0$  at  $N_g = 0$  and  $N_g = \frac{1}{2}$ . It is crucial to capture this boundary condition behaviour in the NRG simulations of the model, since  $dN/dT$  must be integrated over (half of) the whole Coulomb oscillation period to correctly obtain the entropy via the Maxwell relation. Hence one must keep multiple charge states in the model ( $\bar{N} > 1$ ) to capture the correct gate-periodicity of the Coulomb peaks.

At very low temperatures the Coulomb peaks become very narrow such that the minimum conductance  $G_{\min} \simeq 0$  in the middle of the valley. Only in this universal regime can the results of the two-charge-state model be used. The experiments are not in this fully universal regime.

- 
- [1] Sela, E. *et al.* Detecting the universal fractional entropy of majorana zero modes. *Phys. Rev. Lett.* **123**, 147702 (2019).  
[2] Rozhkov, A. Impurity entropy for the two-channel kondo model. *International Journal of Modern Physics B* **12**, 3457–3463 (1998).  
[3] Furusaki, A. & Matveev, K. Theory of strong inelastic cotunneling. *Phys. Rev. B* **52**, 16676 (1995).  
[4] Iftikhar, Z. *et al.* Tunable quantum criticality and super-ballistic transport in a “charge” kondo circuit. *Science* **360**, 5592 (2018).  
[5] Wilson, K. G. The renormalization group: Critical phenomena and the kondo problem. *Rev. Mod. Phys.* **47**, 773 (1975).  
Bulla, R., Costi, T. A. & Pruschke, T. Numerical renormalization group method for quantum impurity systems. *Rev. Mod. Phys.*

- Phys.* **80**, 395 (2008).
- [6] Mitchell, A. K., Galpin, M. R., Wilson-Fletcher, S., Logan, D. E. & Bulla, R. Generalized wilson chain for solving multichannel quantum impurity problems. *Physical Review B* **89**, 121105 (2014).  
Stadler, K., Mitchell, A., von Delft, J. & Weichselbaum, A. Interleaved numerical renormalization group as an efficient multiband impurity solver. *Phys. Rev. B* **93**, 235101 (2016).
- [7] Weichselbaum, A. & von Delft, J. Sum-rule conserving spectral functions from the numerical renormalization group. *Phys. Rev. Lett.* **99**, 076402 (2007).
- [8] E. L. Minarelli and A. K. Mitchell, *in preparation* (2021).
- [9] J. B. Rigo and A. K. Mitchell, *in preparation* (2021).